2540 *Biochemistry* **2010,** *49,* 2540–2550
DOI: 10.1021/bi901933d

BIOCHEMISTRY
including biophysical chemistry & molecular biology
Article

Kinetic and Structural Analysis of Substrate Specificity in Two Copper Amine Oxidases from *Hansenula polymorpha*[†,‡]

Cindy M. Chang,[§,@] Valerie J. Klema,[∥,#] Bryan J. Johnson,[∥,#,▽] Minae Mure,[⊥] Judith P. Klinman,*[,§] and Carrie M. Wilmot*[,∥]

[§]*Department of Chemistry and Department of Molecular and Cell Biology, University of California, Berkeley, California 94720,* [∥]*Department of Biochemistry, Molecular Biology and Biophysics, University of Minnesota, Minneapolis, Minnesota 55455, and* [⊥]*Department of Chemistry, University of Kansas, Lawrence, Kansas 66045* [@]*Current address: LS9, 600 Gateway Blvd., South San Francisco, CA 94080.* [#]*These authors contributed equally to this work.* [▽]*Current address: R&D Systems, Inc., 614 McKinley Place NE, Minneapolis, MN 55413.*

Received November 10, 2009; Revised Manuscript Received February 12, 2010

ABSTRACT: The structural underpinnings of enzyme substrate specificity are investigated in a pair of copper amine oxidases (CAOs) from *Hansenula polymorpha* (HPAO-1 and HPAO-2). The X-ray crystal structure (to 2.0 Å resolution) and steady state kinetic data of the second copper amine oxidase (HPAO-2) are presented for comparison to those of HPAO-1. Despite 34% sequence identity and superimposable active site residues implicated in catalysis, the enzymes vary considerably in their substrate entry channel. The previously studied CAO, HPAO-1, has a narrow substrate channel. In contrast, HPAO-2 has a wide funnel-shaped substrate channel, which also contains a side chamber. In addition, there are a number of amino acid changes within the channels of HPAO-2 and HPAO-1 that may sterically impact the ability of substrates to form covalent Schiff base catalytic intermediates and to initiate chemistry. These differences can partially explain the greatly different substrate specificities as characterized by k_{cat}/K_m value differences. In HPAO-1, the k_{cat}/K_m for methylamine is 330-fold greater than for benzylamine, whereas in HPAO-2, it is benzylamine that is the better substrate by 750-fold. In HPAO-2, an inflated $^{D}k_{cat}/K_m$(methylamine) in relation to $^{D}k_{cat}/K_m$(benzylamine) indicates that proton abstraction has been impeded more than substrate release. In HPAO-1, $^{D}k_{cat}/K_m$(S) changes little with the slow substrate and indicates a similar increase in the energy barriers that control both substrate binding and subsequent catalysis. In neither case is k_{cat}/K_m for the second substrate, O_2, significantly altered. These results reinforce the modular nature of the active sites of CAOs and show that multiple factors contribute to substrate specificity and catalytic efficiency. In HPAO-1, the enzyme with the smaller substrate binding pocket, both initial substrate binding and proton loss are affected by an increase in substrate size, while in HPAO-2, the enzyme with the larger substrate binding pocket, the rate of proton loss is differentially affected when a phenyl substituent in the substrate is reduced to the size of a methyl group.

Copper amine oxidases (CAOs)[1] are virtually ubiquitous in aerobic organisms and catalyze the oxidative deamination of primary amines in the following overall reaction:

$$RCH_2NH_3^+ + O_2 + H_2O \rightarrow RCHO + H_2O_2 + NH_4^+$$

While usually sharing only 20−40% amino acid sequence identity, features of the active sites are almost identical across CAOs from widely varying species. These include the protein-derived enzymatic cofactor, 2,4,5-trihydroxyphenylalanine quinone (TPQ), an active site metal, copper, and its three histidine ligands (*1*, *2*). The CAO mechanism is ping-pong and proceeds via Schiff base chemistry, creating a covalent adduct of the amine substrate with the TPQ (Scheme 1). A conserved Asp residue acts as the catalytic base. The release of aldehyde product at the end of the enzymatic reductive half-reaction leaves the cofactor as a two-electron reduced aminoquinol containing a substrate-derived nitrogen. In the oxidative half-reaction, the reduced enzyme is converted to a one-electron reduced *N*-semiquinone and then an oxidized iminoquinone through the reduction of molecular oxygen to hydrogen peroxide. This is followed by hydrolysis of the iminoquinone to regenerate the resting TPQ quinone and release ammonia.

Despite these similarities, CAOs from different organisms preferentially react with primary amine structures that range from small aliphatic amines to peptides. The CAO from *Escherichia coli*, for example, prefers aromatic monoamines (*3*), while the previously characterized CAO from *Hansenula polymorpha* (HPAO-1) is most active against small aliphatic amines (*4*). The structural basis for this difference in substrate specificity has remained elusive.

[†]This work was supported by National Institutes of Health Grant GM39296 to J.P.K., Grant GM66569 to C.M.W., and Chemistry-Biology Interface Training Grant GM-008700 to B.J.J., National Science Foundation grant MCB-0747377 to M.M., and Minnesota Medical Foundation Grant 3714-9221-06, Office of the Dean of the Graduate School of the University of Minnesota Grant 21087, and a Minnesota Partnership for Biotechnology and Medical Genomics Grant SPAP-05-0013-P-FY06 to C.M.W.

[‡]Coordinates and structure factors have been deposited in the Protein Data Bank as entry 3loy.

*To whom correspondence should be addressed. C.M.W.: telephone, (612) 624-2406; fax, (612) 624-5121; e-mail, wilmo004@umn.edu. J.P.K.: telephone, (510) 642-2668; fax, (510) 643-6232; e-mail, klinman@berkeley.edu.

[1]Abbreviations: CAO, copper amine oxidase; HPAO, *H. polymorpha* copper amine oxidase; TPQ, 2,4,5-trihydroxyphenylalanine quinone; MAO, flavin-containing monoamine oxidase; NBT, nitroblue tetrazolium; ASU, asymmetric unit.

 Published on Web 02/15/2010

Scheme 1: Proposed Reaction Mechanism for HPAO-1, Indicating Intermediates along the Pathway[a]

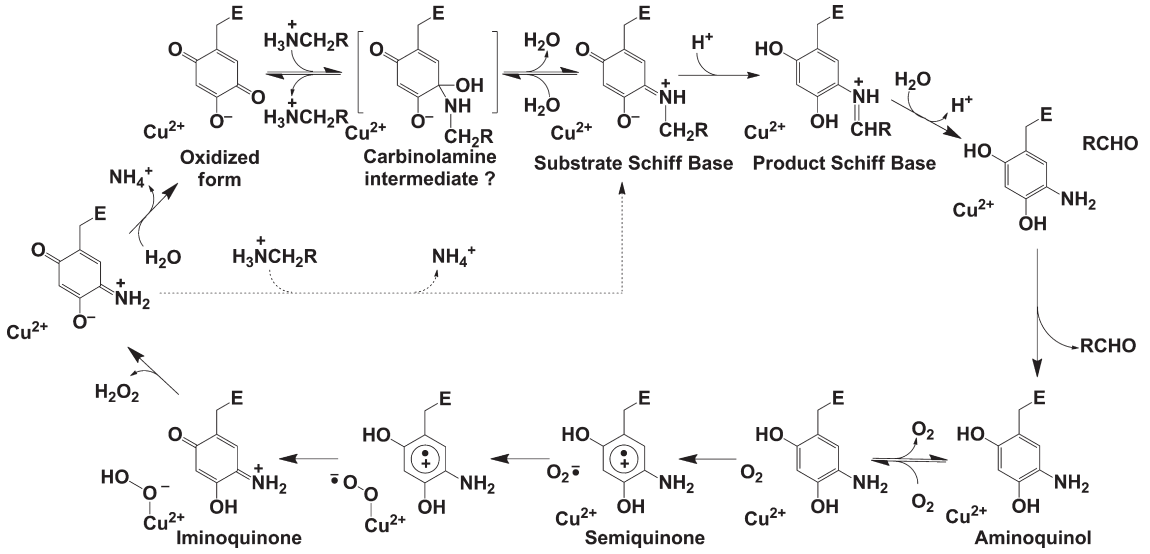

[a]Brackets indicate the probable, but unconfirmed, existence of a carbinolamine intermediate. The dashed arrow indicates that substrate can react directly with the iminoquinone to form the substrate Schiff base when substrate concentrations are high.

Copper amine oxidases are not unique in their variable substrate specificity. Among other classes of enzymes, e.g., aminotransferases (*5*) and flavin-containing monoamine oxidases (MAOs) (*6*), the basis of isoenzyme specificity has been explored. Protein conformational flexibility has been suggested as a source of substrate specificity in aspartate aminotransferase and aromatic amino acid aminotransferase (*7*), whereas differences in static hydrophobic and aromatic $\pi-\pi$ interactions in the substrate binding pocket have been implicated in MAO-A (*8*). It is rare for paralogous enzymes to demonstrate a strong yet inverted discrimination between two different substrates. Thus, most investigations have focused on understanding the relative rates of preferred over poor substrates in a single enzyme, rather than between isoenzymes.

The first described CAO from the methylotrophic yeast *H. polymorpha* (HPAO-1) was heterologously expressed in *Saccharomyces cerevisiae* and purified in 1994 (*4*) and subsequently studied by X-ray crystallography (*9*). Although a peroxisomal protein in its native host organism, it was found in the cytosol of *S. cerevisiae* during recombinant expression (*10*). Characterized as a "methylamine oxidase", HPAO-1 demonstrated much greater activity against methylamine than benzylamine. However, extraction of CAO from *H. polymorpha* grown on benzylamine-enriched media had indicated the presence of a second CAO with a distinct catalytic activity toward benzylamine (*4*). In the case of mammals, multiple CAO isoenzymes have also been established, annotated as *aoc-1*, *aoc-2*, and *aoc-3* in the human genome (*11*). Comparison of the enzymatic activities of the human kidney diamine oxidase (*12*) to human vascular adhesion protein-1 (*13*) indicates broad though largely nonoverlapping substrate specificities. Although these two human enzymes have also been characterized structurally (*14*−*16*), their broad substrate specificities make it difficult to rationalize the features that control substrate discrimination.

In this work, we report detailed kinetic and crystallographic characterization of a second copper amine oxidase from *H. polymorpha* (HPAO-2) for comparison with HPAO-1. In particular, k_{cat}/K_m data indicate a marked reversal of substrate selectivity between the two isoenzymes when their activities are interrogated with a small aliphatic versus an aromatic amine. Using the X-ray crystal structure of HPAO-2 reported here to compare to that of HPAO-1, we can begin to decipher the structural origins of this divergent substrate specificity. Residue changes between HPAO-1 and HPAO-2 that likely play roles in determining substrate specificity have been identified close to the active site and are discussed in the context of the available kinetic parameters and corresponding isotope effects.

MATERIALS AND METHODS

Cloning. Because of the unavailability of the *H. polymorpha* genome at the start of the investigation, the *hpao-2* gene (1967 bp) was cloned out of the *H. polymorpha* genome by "genome walking", using iterations of primers to progressively amplify the entire gene. Initially, mass spectrometry of trypsin-digested protein isolated from cell extracts of *H. polymorpha* grown on benzylamine-enriched growth media that demonstrated CAO activity yielded peptide sequences distinct from that of the original HPAO (HPAO-1). Degenerated primers were designed on the basis of the new peptide sequences, and subsequent PCR resulted in a 600 bp gene fragment of *hpao-2*. The 5′ end and 3′ end sequences of the fragment were then used for upstream and downstream genome walking to yield 1967 bp of the full-length *hpao-2* sequence. The identity of the full-length gene was verified by comparison to the now available *H. polymorpha* genome (Rhein Biotech, personal communication). The *hpao-2* gene was inserted into the *S. cerevisiae* expression vector, pYES2 (Invitrogen), under inducible control by the *GAL1* promoter, via cloned KpnI and XbaI restriction enzyme cut sites present in the multiple cloning site. The full DNA-derived protein sequence and its comparison to HPAO-1 are given in Figure S1 of the Supporting Information.

Expression. Invitrogen's INVSC-1 *S. cerevisiae* cells were transformed with selection for uracil-independent growth, conferred by the *ura3* gene on pYES2. Importantly, *S. cerevisiae* contains no CAO genes and, thus, no background CAO expression. Starter cultures were grown in URA^- minimal medium containing 6.7% yeast nitrogen base without amino acids and 0.77 g/L complete supplemental mixture without uracil

(MP Biomedicals) with 2% raffinose as a carbon source at 30 °C and 225 rpm in a New Brunswick Scientific Innova 4300 temperature-controlled platform shaker. At an OD_{600} of ~5, cells were diluted to an OD_{600} of 0.4 into URA^- minimal medium with 30 μM $CuSO_4$, 1% raffinose, and 2% galactose for induction of expression. Induced cultures were grown in 1.5 L volumes in 4 L flasks. After being induced for 24 h, cells were pelleted by centrifugation in a Sorvall RC 5C Plus centrifuge at 5000 rpm in an SLA-3000 fixed angle rotor for 5 min at 4 °C. Typically, 9 L of cell culture yields 60−70 g of cell pellet.

Purification. Protein purification followed the previously developed purification strategy for HPAO-1 with some modifications (*4*). Cells were lysed with glass beads (425−600 μm, Sigma G8772) in the presence of four protease inhibitors: 0.5 mM phenylmethanesulfonyl fluoride, 5 mM 1,10-phenanthroline, 1 μM pepstatin A, and 5 μM E-64 (Sigma). Approximately 150 mL of glass beads was combined with an ~250 mL suspension of cell pellet and cold 10 mM potassium phosphate (pH 7.2) in a bead beater. Cells were lysed by five cycles of grinding for 5 min and resting for 2 min, with changes in the ice and water surrounding the bead-beating chamber between cycles. The cell extract was then separated from cellular debris by centrifugation in a Sorvall RC 5C Plus centrifuge in ~40 mL aliquots at 12000 rpm in an SS-34 fixed angle rotor at 4 °C for 1 h.

The lysate was loaded onto an ~200 mL (5 cm diameter, ~20 cm height) Q-Sepharose column, pre-equilibrated with 5 mM potassium phosphate (pH 7.2). This column was washed with 1 L of 5 mM potassium phosphate (pH 7.2). Protein was eluted as follows: 300 mL total volume of a linear gradient from 5 to 100 mM potassium phosphate (pH 7.2) followed by 200 mL of 100 mM potassium phosphate (pH 7.2), then a 300 mL total volume of a linear gradient from 100 to 400 mM potassium phosphate (pH 7.2), and finally 300 mL of 400 mM potassium phosphate (pH 7.2). Fractions (10 mL) were collected at a rate of 1 min/fraction (elution by gravity). The column was washed with 1 L of 400 mM potassium phosphate and 1 M NaCl between preparations and then re-equilibrated with ~1 L of 5 mM potassium phosphate (pH 7.2).

Fractions 28−58 were pooled at 4 °C and dialyzed (Pierce SnakeSkin Pleated Dialysis Tubing 10000 MWCO, catalog no. 68100) into 4 L of 50 mM potassium phosphate (pH 7.2) overnight at 4 °C. Dialyzed pooled fractions were then centrifuged at 12000 rpm (1 h at 4 °C) to separate out precipitated protein. Cleared pooled fractions were concentrated to approximately 6 mL using Amicon concentrators with polyethersulfone, 50000 NMWL ultrafiltration membranes.

Aliquots (2 mL) of the concentrated pool were centrifuged at 13000 rpm for 5 min at 4 °C in a benchtop microcentrifuge to clear any precipitation prior to being loaded onto an S-300 column. This was run overnight, by elution with 50 mM potassium phosphate (pH 7.2). Fractions were collected every 10 min at a flow rate of 0.2 mL/min (for ~2 mL/fraction).

Pooled fractions 46−58 were concentrated using an Amicon concentrator with polyethersulfone, 50000 NMWL ultrafiltration membranes. After a final volume of ~2−3 mL had been reached, 50−100 μL aliquots of purified protein were made, snap-frozen in liquid nitrogen, and kept at −20 °C for short-term storage or −80 °C for long-term storage. Concentrated purified HPAO-2 samples were peach in color.

Protein Characterization. The total protein concentration was measured with a Bradford assay (Bio-Rad). Typical total protein yields varied from 150 to 300 mg/9 L of cell culture (at a 90% purity, as judged by SDS−PAGE).

The presence of a quinone cofactor in HPAO-2 was tested by both quinone stain and phenylhydrazine assay. Reaction with phenylhydrazine resulted in the formation of a peak at 448 nm, as previously observed in HPAO-1 (*4*). The very rapid formation of the product phenylhydrazone at room temperature in 100 mM potassium phosphate (pH 7.2) necessitated the use of a Hi-Tech Scientific stopped-flow instrument to estimate a rate constant. The phenylhydrazine assay used a 5-fold molar excess of a freshly prepared solution of phenylhydrazine HCl [in 100 mM potassium phosphate (pH 7.2)] to HPAO-2 protein concentration, as determined by the Bradford assay. The change in absorbance at 448 nm was measured on a Hewlett-Packard 8452A diode array spectrophotometer. An extinction coefficient previously determined for HPAO-1 (40500 M^{-1} cm^{-1}) and a subunit molecular weight of 72000 were used to calculate the percentage of TPQ present in protein (*17*). The presence of TPQ cofactor was also observed by redox stain, specifically via reaction of the protein-bound quinone with nitroblue tetrazolium (NBT) (*17*). After separation of HPAO-2 from contaminants by SDS−PAGE, protein was electroblotted onto a nitrocellulose membrane and washed in the dark with 0.24 mM NBT in 2 M sodium glycinate (pH 10).

Purified HPAO-2 was N-terminally sequenced at the Stanford PAN facility (http://cmgm.stanford.edu/pan/) by Edman degradation.

Kinetic Measurements. Methylamine, [1,1,1-$^2H_3$]methylamine, and benzylamine hydrochlorides were purchased from Sigma and used without further purification. [1,1-$^2H_2$]Benzylamine hydrochloride was prepared as previously described (*18*). The purity of synthesized [1,1-$^2H_2$]benzylamine hydrochloride and commercial [1,1,1-$^2H_3$]methylamine were verified by NMR with no evidence of contamination by protium substrate found. In all cases with protio and deuterio substrates, NMR spectra also indicated no significant level of chemical contaminant.

Observation of the formation of benzaldehyde from benzylamine (*19*) served as a preliminary enzyme activity assay during the purification of HPAO-2 and in subsequent kinetic studies of benzylamine. Benzaldehyde absorbs at 250 nm (ε = 12800 M^{-1} cm^{-1}), and its production is easily followed on a Hewlett-Packard 8452A diode array spectrophotometer. Enzyme activity with a varying level of methylamine was monitored by oxygen consumption with a Clark oxygen electrode. Unless otherwise noted, all kinetic studies were conducted at 25 °C in 100 mM potassium phosphate (pH 7.2), controlled for an ionic strength of 300 mM by the addition of KCl (*4*). In HPAO-2 assays, the range of concentration for amine substrates was 0.5−20 mM for methylamine and 1−200 μM for benzylamine. In HPAO-1, 0.05−1.5 mM methylamine and 0.2−5 mM benzylamine were used for steady state kinetic rate parameter determination. Buffers used for the pH studies were 100 mM potassium phosphate (pH 6.2−8.2), 25 mM sodium pyrophosphate (pH 8.6), and 0.1 M potassium carbonate (pH 9.2−9.5) (Sigma). Ionic strength was maintained at 300 mM with KCl for potassium-based buffers and NaCl for sodium-based buffer. These studies were conducted at 1−150 μM benzylamine at 25 °C. Enzyme activity at a varying level of oxygen, at saturating amine concentrations, for determination of $k_{cat}/K_m(O_2)$ values was monitored by oxygen consumption with a Clark type oxygen electrode. The kinetic parameters, k_{cat} and k_{cat}/K_m, were derived

from data fit to the Michaelis−Menten equation by nonlinear regression using Kaleidagraph (Abelbeck Software).

Crystallization. HPAO-2 in 50 mM potassium phosphate (pH 7.2) was buffer exchanged into 20 mM HEPES (pH 7.0) and concentrated to 23 mg/mL for crystallization. HPAO-2 crystals were grown by sitting drop vapor diffusion using a 1:1 volume ratio (6 μL total) of purified HPAO-2 and a mother liquor solution [0.50−0.75 M potassium sodium tartrate tetrahydrate in 0.10 M phosphate (pH 6.0−7.5)] at 20 °C. Crystals grew as clusters, and physical manipulation was necessary to separate individual crystals. Crystals were soaked in 25% high-purity glycerol (Hampton Research) mixed with mother liquor taken directly from the crystallization well for 5 min prior to being flash-frozen in liquid nitrogen.

Structure Determination and Refinement. X-ray diffraction data were collected from a single crystal at 100 K using an undulator source (wavelength of 0.979 Å) and an ADSC Quantum 315r detector at the Advanced Photon Source, Argonne National Laboratory (beamline 19-ID, SBC-CAT). Data were processed using HKL2000 and SCALEPACK (*20*). Molecular replacement was conducted using PHASER and MOLREP from the CCP4 suite (*21*) with a polyalanine truncated search model based on a previously deposited HPAO-1 model [Protein Data Bank (PDB) entry 2oov] (*22*).

An initial model was built into the experimental electron density, and manual adjustments were made in Coot (*23*). Model refinement was performed using Refmac5 with 5% of the data excluded from the refinement to enable calculation of R_{free} (*24*). ARPWaters was used to place water molecules into the model at peaks greater than 3.0σ in the $2F_o - F_c$ map (*25*). Cycles of model building and refinement were performed until $F_o - F_c$ difference peaks did not make structural sense and appeared to be within the noise level of the electron density map.

RESULTS

Characterization of HPAO-2 and Comparison to HPAO-1. Cell extracts after induction for 24 h contained a band at ~72 kDa that is absent in the nontransformed control yeast cell extracts. The size of the protein corresponds to the estimated size of HPAO-2 calculated from the primary sequence. After purification, the resulting protein constituted >90% of the total protein, as observed by SDS−PAGE (Figure S2 of the Supporting Information). The net effect of the purification protocol was to increase the relative amounts of HPAO-2 to the contaminant bands. Some of the contaminant bands also stained on an NBT blot, indicating probable breakdown of HPAO-2 (data not shown). HPAO-1 migrates slightly faster by SDS−PAGE, suggesting an overall smaller primary structure; however, the DNA-derived primary protein sequence of HPAO-1 predicts a protein slightly larger than HPAO-2. Post-translational modifications may account for this difference as HPAO-2 has an additional predicted glycosylation site. Concentrated purified HPAO-2 was a vibrant peach color, characterized by a broad shoulder in the UV−vis region around 480 nm (Figure 1). N-Terminal sequencing of the protein matched the expected N-terminus from the HPAO-2 DNA sequence, except for the absence of the initial Met (Figure S3 of the Supporting Information). The N-terminus of HPAO-1 is longer by 20 amino acids and contains a peroxisomal targeting sequence (Figure S3 of the Supporting Information).

The presence of a quinone cofactor was tested by both quinone stain and phenylhydrazine assay. Nitroblue tetrazolium staining

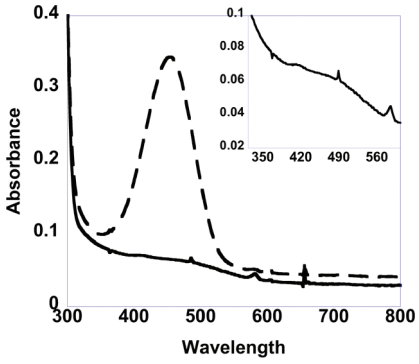

FIGURE 1: UV−visible spectra of 20 μM HPAO-2 before (—) and after (− − −) incubation for 5 min with 100 μM phenylhydrazine HCl in 100 mM potassium phosphate buffer (pH 7.2) at 25 °C. The inset shows 20 μM HPAO-2 before incubation with phenylhydrazine HCl blown up to show a shoulder at 480 nm, as observed for other TPQ-containing enzymes.

resulted in a purple band similar to that observed with HPAO-1 (data not shown). Reaction with phenylhydrazine resulted in the rapid formation of a peak in the region seen previously with other CAOs (~450 nm) corresponding to the phenylhydrazone (Figure 1). The rate of phenylhydrazone formation in HPAO-2 (87 ± 3 s^{-1}) is $>10^4$-fold faster than that of HPAO-1 ($7.8 \times 10^{-3} \pm 7.0 \times 10^{-4}$ s^{-1}). Typical yields of phenylhydrazone correspond to ~50% of the subunit concentration.

The copper content of purified protein was measured by elemental analysis. Initial analyses indicated 2 mol of copper per monomer. However, after overnight dialysis against 1 mM EDTA, followed by dialysis against 0.1 M potassium phosphate buffer (pH 7.2), the expected level of one copper per monomer was observed. The presence of the loosely bound second copper did not affect enzyme turnover rates, as kinetic measurements performed with the dialyzed enzyme yielded rates that were the same as those with nondialyzed enzyme samples (Table S1 of the Supporting Information). Thus, there appears to be an adventitious metal binding site that plays no role in catalysis.

Kinetic Properties. The near-unity $^{D}k_{cat}$ values observed for HPAO-2 with both substrates indicate that proton abstraction is not significantly rate-limiting with either substrate (Table 1). The lower limit for the rate constant reflecting the proton abstraction step is thus defined by the respective k_{cat} values. Conversely, HPAO-1 has an elevated $^{D}k_{cat}$ for the slower substrate benzylamine [$^{D}k_{cat}$(benzylamine) equals 5.9, whereas $^{D}k_{cat}$(methylamine) equals 1.7], pointing to a higher relative energy barrier for proton loss from the poor substrate relative to other steps following substrate binding. The overall turnover rate (k_{cat}) for benzylamine is also down 94-fold relative to that for methylamine. Stopped-flow kinetic studies of HPAO-1 have confirmed the oxidative half-reaction is the major determinant of rate during turnover with methylamine (*26*).

Overall, the changes in k_{cat} between the different amine substrates are smaller than the changes in k_{cat}/K_m(S) (Table 1). The second-order rate constant reflects turnover under low substrate conditions and varies by 750-fold between the two substrates for HPAO-2. The change in k_{cat}/K_m(S) between substrates observed with HPAO-1 is similar, but somewhat smaller (330-fold). As such, HPAO-2 shows a clear preference for bulkier aromatic amines, and HPAO-1 shows a preference for short aliphatic amines. These differences in k_{cat}/K_m(S) originate from substrate-dependent rate differences in one or more steps

Table 1: Steady State Kinetic Parameters for HPAO-1 and HPAO-2 at 25 °C in 100 mM Potassium Phosphate (pH 7.2) with the Ionic Strength Maintained at 300 mM with KCl

	k_{cat} (s^{-1})	$k_{cat}/K_m(S)^a$ (M^{-1} s^{-1})	$k_{cat}/K_m(O_2)^b$ (M^{-1} s^{-1})	$^Dk_{cat}$	$^Dk_{cat}/K_m(S)$
			HPAO-2		
benzylamine	8.1 ± 0.2	$(9 \pm 1) \times 10^5$	$(4.7 \pm 0.6) \times 10^5$	1.00 ± 0.04	2.0 ± 0.3
methylamine	2.18 ± 0.06	$(1.2 \pm 0.1) \times 10^3$	$(1.6 \pm 0.3) \times 10^5$	1.36 ± 0.08	18.5 ± 0.1
			HPAO-1		
benzylamine	$(6.6 \pm 0.3) \times 10^{-2}$	$(9 \pm 1) \times 10$	$(8.1 \pm 2.1) \times 10^4$	5.9 ± 0.7	3 ± 1
methylamine[c]	6.2 ± 0.2	$(3.0 \pm 0.6) \times 10^4$	$(4 \pm 1) \times 10^5$	1.7 ± 0.1	4.3 ± 0.2

[a]Amine substrate. [b]Measured at saturating amine substrate and varying oxygen levels. This led to some variation in ionic strength: HPAO-2, μ = 250 mM with benzylamine and μ = 300 mM with methylamine; HPAO-1, μ = 257 mM with benzylamine and μ = 250 mM with methylamine. [c]Data from ref *26*; experimental conditions identical to those herein, except at pH 7.0 instead of pH 7.2.

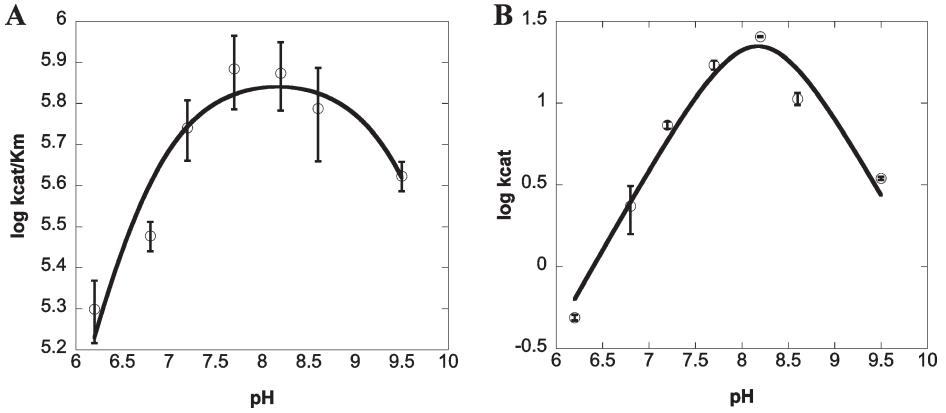

FIGURE 2: HPAO-2 pH profiles of (A) k_{cat}/K_m(benzylamine) (pK_{a1} = 6.6, and pK_{a2} = 9.7) and (B) k_{cat} (pK_{a1} = 6.0, pK_{a2} = 7.6, and pK_{a3} = 8.9).

Scheme 2: Proposed Free Energy Diagrams That Represent k_{cat}/K_m(S) for (A) HPAO-2 and (B) HPAO-1

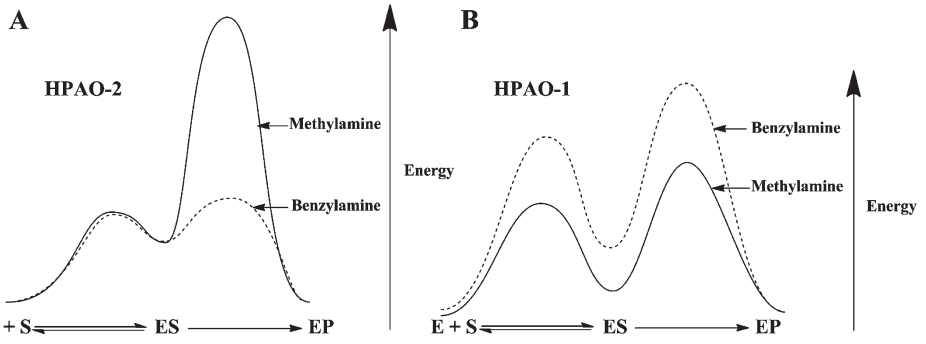

that occur between binding of the substrate to the enzyme up to and including the first irreversible step (Scheme 1).

In contrast, $k_{cat}/K_m(O_2)$ changes little between the two substrates and two isoenzymes (Table 1). This suggests that steps from oxygen binding through the irreversible oxygen reduction step vary little between the two substrates, as expected for the ping-pong mechanism proposed for HPAO-1 (Scheme 1). The small reduction in $k_{cat}/K_m(O_2)$ for methylamine turnover (as compared to that of benzylamine) in HPAO-2 could suggest oxygen binding to an enzyme form that has retained formaldehyde and is unreactive to O_2 until the product is released. Bound aldehyde product has been shown to significantly impede the oxidative half-reaction in *E. coli* CAO crystals, where the restraints imposed by the lattice lead to very slow product release (*27*).

Comparison of isotope effects on k_{cat}/K_m(S) on the two isoenzymes with both substrates demonstrates that the extent of rate limitation by proton abstraction differs on steps in the reductive half-reaction. Isotope effects on k_{cat}/K_m(S) with HPAO-2 indicate that proton abstraction is clearly more rate-limiting for methylamine than benzylamine, as $^Dk_{cat}/K_m$(S) equals 2.0 for benzylamine and 18.5 for methylamine (Table 1). The increase in the contribution of the proton abstraction step to k_{cat}/K_m is likely due to an increase in the free energy barrier for proton abstraction, rather than a decrease in the barrier for methylamine binding (Scheme 2A), as this substrate is smaller than the preferred substrate benzylamine and thus should have no trouble accessing the active site. In the case of HPAO-1, the similar $^Dk_{cat}/K_m$ values [3.0 for benzylamine vs 4.3 for methylamine (Table 1)] indicate that proton abstraction is similarly rate-limiting with respect to substrate binding for both substrates, despite the large reduction in rate when using benzylamine as the substrate. This implies that both substrate binding/release

and proton abstraction are affected to a similar extent (Scheme 2B).

The impact of pH on catalysis has also been examined for HPAO-2 (benzylamine as the substrate) for comparison to that of HPAO-1 [methylamine as the substrate (*28*)]. As summarized in Figure 2, the pH optima for both $k_{cat}/K_m(S)$ and k_{cat} are ~8−8.2 and similar to that of HPAO-1 (*28*). The fact that these pH optima are elevated above pH 7 is consistent with the fact that HPAO-1 is found in the peroxisome with a pH of 8.2 in *S. cerevisiae* (*29*). The intracellular location of HPAO-2 is unknown; however, the absence of an extended N-terminus in relation to HPAO-1 suggests the site of function may be cytosolic (Figure S3 of the Supporting Information).

Crystal Structure of HPAO-2 in Comparison to That of HPAO-1: Overall Fold and Active Site. Table 2 contains the data collection, processing, and refinement statistics for HPAO-2 to a resolution of 2.0 Å. Final R_{work} and R_{free} values are 14.5 and 19.1%, respectively (for the quality of the electron density, see Figure S4 of the Supporting Information). Three polypeptide chains, or 1.5 physiological HPAO-2 dimers, were seen in the crystallographic asymmetric unit (ASU) in space group *C*2. The overall structure of the HPAO-2 dimer is identical in fold to that of HPAO-1 and other CAOs (Figure 3 and Figure S5 of the Supporting Information) (*2*, *9*, *14*−*16*, *30*−*33*). Superimposition of the HPAO-2 and HPAO-1 homodimer yields a root-mean-square deviation (rmsd) for main chain atoms of 0.99 Å (Figure S6 of the Supporting Information). HPAO-2 consists of three domains arranged along its primary sequence (D2−D4). The amine oxidase from *E. coli* contains an additional protruding "stalk" domain (D1) at the N-terminus that is not present in the other CAO crystal structures (*2*). Two small α/*β* domains (D2 and D3) are formed by the N-terminal portion of HPAO-2, while the larger catalytic domain (D4) is composed of the C-terminal portion of the chain. As seen in HPAO-1, the catalytic domain (D4) of HPAO-2 contains a complex antiparallel *β*-sandwich fold (*9*). Two *β*-hairpin arms protrude from each monomer and form part of the intricate interaction within the HPAO-2 homodimer (Figure 3). Some CAOs from different sources, such as *E. coli*, pea seedling, and human kidney, bind a calcium or manganese ion at an additional site on the periphery of the protein (*2*, *12*, *16*, *31*). Like HPAO-1, no evidence of this second metal binding site was observed in the HPAO-2 crystal structure (*9*). Unusually, an adventitious second copper ion is present in HPAO-2 samples following initial protein purification. Even though the protein used in crystallization had not been dialyzed against EDTA, which removes this loosely bound copper, there was no evidence in the electron density to indicate where this site may be located within the protein. HPAO-2 contains eight cysteine residues per monomer, but only two form a disulfide bond (Cys 321 and Cys 347). In HPAO-1, the two equivalent cysteine residues (12 Cys residues in total) also form the single disulfide bond of HPAO-1 (Cys 338 and Cys 364) (*9*).

The HPAO-2 active site is deeply buried within the protein interior. The two active sites within the functional HPAO-2 homodimer each contain a TPQ cofactor (42.2 Å between the C_α atom of each TPQ cofactor) and a cupric ion (34.7 Å between coppers in the dimer) coordinated by three conserved histidine ligands in a distorted square pyramidal geometry (Figure 4). Two well-ordered water molecules are ligated to the copper ion: one sits in an axial position (W_a) bridging O2 of TPQ and the copper and the other in an equatorial position (W_e) nearly planar with the Cu^{2+} and nitrogen atoms of its three histidine ligands

Table 2: X-ray Crystallographic Data Collection, Processing, and Refinement Statistics for HPAO-2

Data Collection and Processing Statistics	
detector type	ADSC Quantum 315r
beamline and source	19-ID SBC-CAT, Advanced Photon Source
temperature (K)	100
space group	*C*2
unit cell dimensions	a = 288.5 Å, b = 91.1 Å, c = 151.1 Å, β = 117.2°
no. of molecules in the unit cell, Z	6
wavelength (Å)	0.9785
resolution (Å)[a]	50.0−2.0 (2.07−2.00)
no. of unique reflections	210228
completeness (%)[a]	90.6 (69.3)
R_{merge}[a,b]	0.089 (0.319)
$I/\sigma I$[a]	13.4 (3.0)
redundancy[a]	3.5 (3.1)
Crystallographic Refinement and Model Statistics	
resolution range (Å)[a]	37.4−2.00 (2.06−2.01)
no. of reflections in the working set[a]	200161 (10684)
no. of reflections in the test set[a]	10514 (539)
R_{work} (%)[a,c]	14.5 (21.9)
R_{free} (%)[a,d]	19.1 (27.3)
no. of non-hydrogen atoms	
no. of amino acid residues	1899
no. of protein atoms	15321
no. of solvent molecules	3199
no. of Cu^{2+} ions	3
no. of other atoms	91
rmsd from ideal geometry	
bond lengths (Å)	0.026
bond angles (deg)	2.0
Ramachadran plot	
energetically favored regions (%)	89.2
additionally allowed regions (%)	10.4
generously allowed regions (%)	0.2
disallowed regions (%)	0.2
average B factor (Å^2)	
main chain	24.4
side chain	26.3
ligands	43.8
solvent atoms	44.2

[a]Numbers in parentheses refer to the highest-resolution shell. [b]$R_{merge} = \sum_{hkl}\sum_i|I_{hkl,i} - \langle I_{hkl}\rangle|/\sum_{hkl}\sum_i I_{hkl,i}$, where I is the observed intensity and $\langle I\rangle$ is the average intensity for multiple measurements. [c]$R_{work} = \sum||F_o| - |F_c||/\sum|F_o|$, where $|F_o|$ is the observed structure factor amplitude and $|F_c|$ is the calculated structure factor amplitude for 95% of the data used in refinement. [d]R_{free} and R_{factor} based on 5% of the data excluded from refinement.

(Figure 4). This latter solvent position is variably occupied in different CAO crystal structures and when modeled has a higher average B factor than the axial water. W_e was clearly observed in all three subunits within the crystallographic ASU of the HPAO-2 electron density, whereas it was only modeled in two of the six subunits in the HPAO-1 structure ASU; thus, this water appears to be more labile in HPAO-1 than HPAO-2 (*22*). The electron density for TPQ clearly indicates that >90% of the active sites in the crystal contain fully formed TPQ (Figure 4), even though treatment with phenylhydrazine of the protein preparation used in crystallization indicated only ~50% TPQ was present. However, the observation of only 50% TPQ could arise from half-of-sites reactivity, which is known to occur in other CAOs, and as indicated in the crystal structure, the true TPQ content could

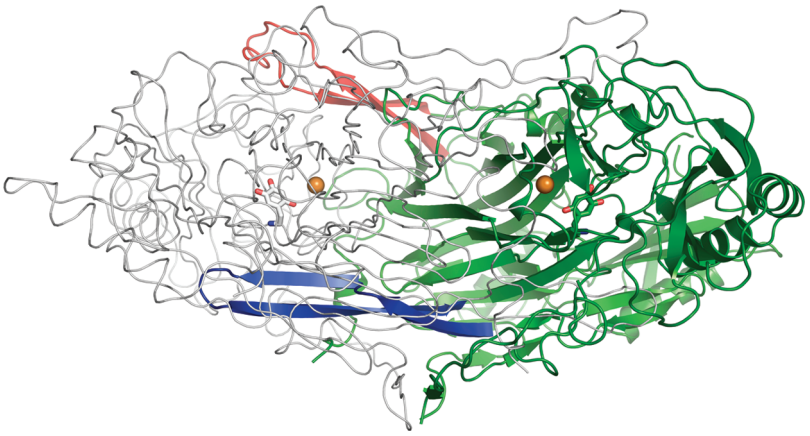

FIGURE 3: Overall view of the HPAO-2 dimer highlighting the two β-hairpin arms. One monomer is displayed as a green ribbon, except for the two β-hairpin arms that are colored blue (corresponding to residues 348−376) and red (corresponding to residues 454−481). The second monomer is displayed as a gray C_α trace. The TPQs are drawn in stick colored by atom type, and copper atoms are displayed as gold spheres. This figure was produced using PyMOL (http://www.pymol.org/).

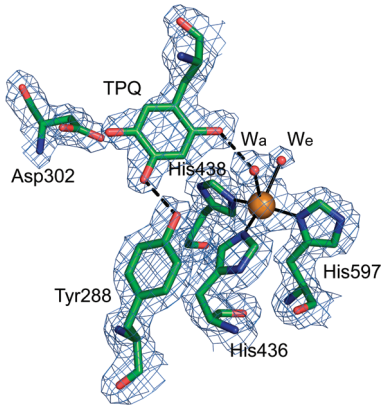

FIGURE 4: Active site of HPAO-2 with $2F_o - F_c$ electron density. Residues are colored by atom type (carbon, green). Hydrogen bonds are indicated by dashed lines. Ligand−metal interactions are indicated by solid lines. The copper ion is shown as a gold sphere. Water molecules are depicted as red spheres (W_a indicates the axial water ligand to the copper and W_e the equatorial water ligand). The $2F_o - F_c$ electron density contoured at 1.5σ is shown as a blue mesh. This figure was produced using PyMOL (http://www.pymol.org/).

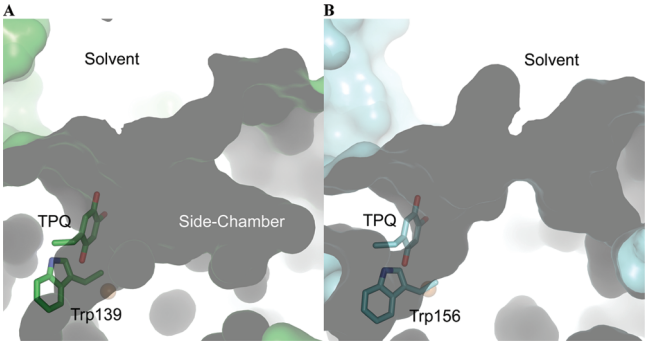

FIGURE 5: Surface representation of substrate entry channels in (A) HPAO-2 and (B) HPAO-1. TPQ and the "gating" Trp are drawn in stick colored by atom type [(A) carbon, green; (B) carbon, blue], and copper is depicted as a gold sphere. This figure was produced using PyMOL (http://www.pymol.org/).

actually be close to 100% (*34*−*36*). Alternatively, enzyme with TPQ in both subunits may have selectively crystallized from the mother liquor. The TPQ cofactor adopts a single orientation with its O2 atom closest to the copper center and O5 atom closest to the conserved catalytic base, Asp302. It is thus poised for substrate attack at C5 to form the substrate Schiff base intermediate and represents a conformation competent for catalysis termed "copper off". There is no evidence of the "copper on" conformation in which O4 of TPQ is directly ligated to the copper displacing the axial water ligand (W_a). This conformation is considered not competent for catalysis as the C5 is inaccessible to amine substrate but is often present in CAO crystal structures, including HPAO-1 where it forms ~30% of the TPQ conformers (*22*).

Crystal Structure of HPAO-2 in Comparison to HPAO-1: Substrate Amine Entry Channel. Although the residues important for chemistry are structurally identical between HPAO-2 and HPAO-1, the substrate channels differ considerably. HPAO-2 has a broad, funnel-shaped substrate entry channel compared to HPAO-1 (Figure 5). The widening of the channel mouth of HPAO-2 is primarily due to a two-residue deletion in the loop of the β-hairpin arm from the other monomer that reaches across close to the active site (blue in Figure 3). This arm contains a conserved His (residues 359 and 376 in HPAO-2 and -1, respectively) that forms a hydrogen bond to the conserved acidic residue following TPQ in the protein sequence. In HPAO-1, the loop is defined by the Arg 380-Asp-Asn-Phe-Ala-Thr 385 sequence, whereas in HPAO-2, the Phe and Ala residues are deleted to give a four-residue β-hairpin turn consisting of Arg 363, Thr 364, Asn 365, and Val 366 (orange in Figure 6). Interestingly, HPAO-2 also has a side chamber just below the mouth of the main channel, which is sufficiently large to accommodate and retain a bulkier aromatic substrate like benzylamine or the outgoing product of its reaction, benzaldehyde (Figure 5 and Figure S7 of the Supporting Information). The chamber is accessed by a mouth that widens out to a diameter of 5.1 Å and is 5.4 Å deep. The chamber has three small pockets at its deepest point that present backbone polar groups (Ile 33, Gln 34, and Ile 35) that could form hydrogen bonds to a substrate amine group (red in Figure 6, and Figure S7A of the Supporting Information). One side of the chamber is hydrophobic, which is formed by the alkyl chain of Arg 332, Val 259, and Ala 310, and would enable a favorable interaction with an aromatic moiety (red except Ala 310 which is blue in Figure 6, and Figure S7B of the Supporting Information). Interestingly, the opposite wall contains a high density of oxygen atoms, which gives a slight negative electrostatic potential to this side of the chamber.

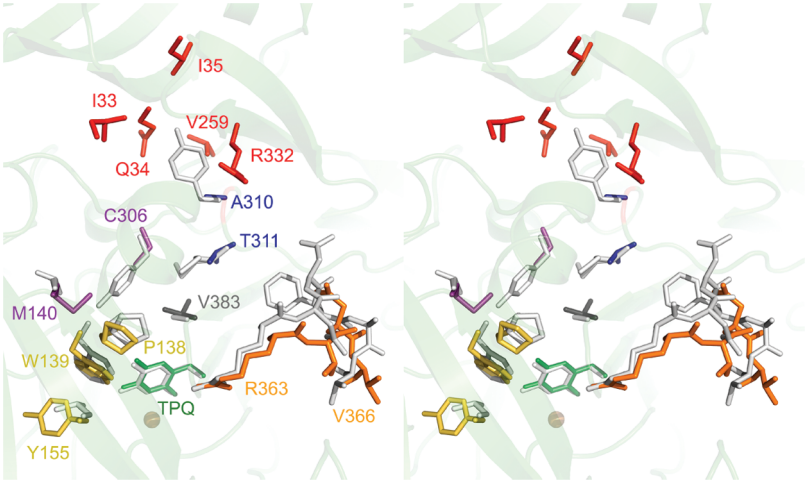

FIGURE 6: Stereo overlay between key residues in HPAO-2 and HPAO-1 that define the substrate channel. Only HPAO-2 residues are numbered, and the side chains are colored as specified in the text. The structurally corresponding residues in HPAO-1 are drawn as white sticks, except in the case of the red HPAO-2 side chains that define the side chamber, which is absent in HPAO-1. The fold of HPAO-2 is depicted as a green ribbon. This figure was produced using PyMOL (http://www.pymol.org/).

Table 3: Differences in Residues between HPAO-2 and HPAO-1 That Likely Impact Accommodation of Substrate and Catalytic Intermediate Structures

HPAO-2	HPAO-1
Met 140	Thr 157
Tyr 155	Leu 174
Cys 306	Tyr 323
Ala 310	Tyr 327
Thr 311	Met 328
Val 383	Ala 402

Between the side chamber and the active site, there are two key sequentially adjacent residue side chain changes that widen the HPAO-2 channel from that of HPAO-1, these being Ala 310 and Thr 311 in HPAO-2 compared to Tyr 327 and Met 328 in HPAO-1 (Table 3, blue in Figure 6).

At the base of the substrate entry channel, where the substrate undergoes chemistry to form the product, there is a conserved Trp in HPAO-2 and -1 [Trp 139 and Trp 156, respectively (Figure 5 and yellow in Figure 6)] that in other CAOs is generally a Tyr or Phe (*2*, *9*, *14*, *15*, *30*−*33*). This residue has been termed a gate to the active site (*33*). It has two major conformers: one blocking access to TPQ (normally observed in resting state CAO crystal structures, although the side chain can also be disordered) and the other rotated out of the way (observed in Schiff base intermediates generated in an active site base mutant, and suicide inhibitor complexes that mimic Schiff base intermediates) (*15*, *36*−*38*). Interestingly, the gate hypothesis does not appear to pertain to mammalian CAOs. The corresponding tyrosine residues in structures of CAO from bovine plasma, human diamine oxidase, and human vascular adhesion protein-1 are in an intermediate position halfway between the "open" and "closed" conformations (*14*−*16*, *32*). In the case of HPAO-2 and -1, both of which have Trp at this position, the gate is always open in these structures, with Trp B-factors that are equivalent to those of surrounding residues indicating a lower mobility than in other CAOs. However, the angle of the Trp side chain is different between the two enzymes, and the main chain is shifted such that the channel in HPAO-1 is more constricted than in HPAO-2 (Figure 5). This appears to primarily result from the substitution of Leu 174 in HPAO-1 for Tyr 155 in HPAO-2 (Table 3 and yellow in Figure 6). This residue does not directly form part of the channel wall but sits behind the five-membered ring of Trp, pushing it into the channel in HPAO-1. The conserved Pro residue that is N-terminal to the Trp in both structures rigidifies the main chain, reducing the possibility of compensating flexibility in the channel (yellow in Figure 6). On the other side of the channel, the main chain is also moved inward in HPAO-1, constricting the channel compared to HPAO-2. This is again a "knock-on" effect due to a two-residue insertion into the tip of the β-hairpin that reaches across from the other monomer of the homodimer and was discussed above (blue in Figure 3 and orange in Figure 6). HPAO-1 has a two-residue insertion (Phe 383-Ala 384) compared to HPAO-2, and it is the side chain of Phe 383 that pushes the main chain containing Ala 402 (Val 383 in HPAO-2) into the substrate channel (Table 3 and colored dark gray in Figure 6). Although Val 383 is a larger side chain than Ala 402, the displacement of the main chain places the end of these two residue side chains at the same place, but the effect N-terminal to these residues is an overall displacement constricting the HPAO-1 channel. The coincident positioning of the end of the side chains of Val 383 in HPAO-2 and Ala 402 in HPAO-1 appears to have an important role, as TPQ is sequentially close to this position (HPAO-2, position 386; HPAO-1, position 405) and the structures become coincident immediately C-terminal to Val 383 or Ala 402.

Finally, there are two side chain changes between HPAO-2 and -1 within the substrate entry channel that would interact with bulky R groups during the reductive half-reaction; in HPAO-2, Met 140 and Cys 306 have replaced Thr 157 and Tyr 323, respectively, in HPAO-1 (Table 3 and magenta in Figure 6).

DISCUSSION

HPAO-2 is the second copper amine oxidase to be isolated and characterized from *H. polymorpha*. The marked change in substrate specificity is largely manifested in k_{cat}/K_m, which is 750-fold greater for benzylamine than methylamine. Complementarily, the k_{cat}/K_m values for the previously studied CAO from the same organism, HPAO-1, are opposite in specificity. Hence, the isolation and characterization of two copper amine

oxidases from the same organism with 67% sequence homology and 34% sequence identity, but inverted substrate specificities, begin to address the nature of substrate specificity in these kinetically diverse enzymes.

The substrate entry and binding pockets of the two enzymes are clearly very structurally different as determined by comparison of the X-ray crystal structures (Figure 5). The wider mouth of the entry channel of HPAO-2 would be more likely to capture and funnel the larger benzylamine from bulk solvent into the heart of the enzyme. In HPAO-1, the channel is almost as narrow at its entrance as it is close to the active site. This would restrict the orientations in which bulky aromatic substrates could enter the channel, which is likely to reduce their probability of capture.

In the amine entry channel in HPAO-2, there is a defined side chamber (Figure 5A). This chamber could easily accommodate benzylamine, and the three pockets at the deepest part of the chamber have polar groups that could form hydrogen bonds with the amine group of substrate (Figure S7 of the Supporting Information). This could be considered a holding area or "anteroom" that increases the local concentration of substrate near the active site. It is also possible that binding of substrate into this side chamber away from the main portion of the entry channel could facilitate movement of the product out of the enzyme. Interestingly, there has been another anteroom identified in CAOs that is proposed to have a similar function, but in this case for substrate O_2 (*22*, *30*, *32*). This anteroom lies on the opposite side of the copper from the amine entry channel and is structurally conserved among CAOs. In contrast, the amine anteroom appears to be a particular feature of HPAO-2 and is unlikely to play a significant role in the kinetics of the enzyme.

The large changes in k_{cat}/K_m between the substrates of both enzymes suggest that substrate binding at the site of chemistry plays a role in determining substrate preference. However, selection against the smaller substrate methylamine for HPAO-2 cannot depend on sterics alone, since the substrate-binding pocket could accommodate both substrates. During catalysis, the formation of tetrahedral intermediates is postulated through nucleophilic attack on C5 of cofactor, as in the initial attack of amine to form the substrate Schiff base (Scheme 1). TPQ in its active "copper-off" conformation sits in a wedge-shaped environment in which the C2−C3 side of the ring forms tight packing interactions with the protein, while the C5−C6 side of the ring does not. This additional space next to C5 is proposed to be important for the accommodation of tetrahedral intermediates during nucleophilic attack (*39*). The C5 environment is controlled primarily by two invariant residues, the Asp catalytic base and the Asn residue (position 385 in HPAO-2 and position 404 in HPAO-1) N-terminal to TPQ. The headgroup of the Asn packs against one face of the TPQ ring, meaning that amine attack can occur only from the other face of the ring that lies by the catalytic base (Figure S8 of the Supporting Information). The importance of this residue in orienting the TPQ cofactor has been demonstrated. Mutation of Asn 404 to Ala in HPAO-1 leads to the accumulation of product Schiff base upon reaction with methylamine (*40*). However, for bulkier substrates, such as benzylamine, the orientation of amine attack and the accommodation of subsequent Schiff base intermediates are controlled by the next sphere of residues that line the entry channel just outside the catalytic active site. A key pair of residues are juxtaposed spatially with the large/small residue pattern being reversed in the two enzymes; Met 140 and Cys 306 in HPAO-2 are replaced with Thr 157 and Tyr 323, respectively, in HPAO-1 (Table 3, magenta in Figure 6, and Figure S9 of the Supporting Information). This has the effect of moving the position of a small pocket such that bulkier R groups can access the HPAO-2 active site. Benzylamine, as a substrate, is unusual in that its product Schiff base is fully conjugated and thus planar, and the shape of the HPAO-2 substrate channel by the active site is more complementary to this species than that of HPAO-1 (Figure S9 of the Supporting Information).

In HPAO-2, the effect of substrate deuteration on k_{cat}/K_m is of particular value in understanding the reduced reactivity with methylamine, specifically the large $^{D}k_{cat}/K_m$ for methylamine as compared to the more optimal substrate, benzylamine. The magnitude of the methylamine $^{D}k_{cat}/K_m$ (18.5 ± 0.1) is very close to the intrinsic isotope effect for CAOs (*41*), implying that proton abstraction has become rate-limiting for the poor substrate. The origin of the reduced k_{cat}/K_m(S) value is thus attributed in part to an impaired proton abstraction step (Scheme 2A). Considering the shape complementarity for benzylamine in the entry channel of HPAO-2, a preferential decrease in the rate of proton abstraction is likely due to difficulty in achieving a precise alignment between the methylamine substrate Schiff base and the active site base. It was also possible that the faster benzylamine rate could reflect an increased level of conjugation in its resulting carbanion−product Schiff complex. However, a comparison of k_{cat}/K_m(S) for the aromatic phenylethylamine oxidation (2.6×10^5 M^{-1} s^{-1}) at the nonconjugated C1 position to the benzylamine value (Table 1) indicates a similar or elevated value.

Although the HPAO-1 and -2 structures overlay exactly with regard to the positions of the catalytic Asp base, copper-off TPQ, and the ordered water molecules between them, TPQ appears to have a lower mobility in HPAO-2 than in HPAO-1. This is supported by the fact that in the three subunits of the crystallographic ASU of HPAO-2 there is no evidence of the copper-on conformer of TPQ, whereas in four of the six subunits in the HPAO-1 structure, there is a substantial proportion of copper-on. The side chain *B* factors of the cofactor and surrounding residues, normalized to the overall *B* factor of each structure, also support the idea that TPQ is less mobile in HPAO-2 than in HPAO-1. This feature may exacerbate the ability of HPAO-2 to orient the reactive carbon of the methylamine Schiff base with the catalytic Asp. We note that there is some isotope effect on k_{cat}/K_m for benzylamine with HPAO-2, indicating that proton abstraction contributes to k_{cat}/K_m for this substrate as well as for methylamine. It is, therefore, very likely that additional factors contribute to the 10^3-fold rate reduction with methylamine oxidation by HPAO-2.

In the case of HPAO-1, similar $^{D}k_{cat}/K_m$ values are observed for both substrates, while the second-order rate constant is reduced ~330-fold for benzylamine. The most likely explanation is that both proton abstraction and substrate binding/release are slowed when the enzyme is challenged with the larger substrate (Scheme 2B). The increase in rate limitation by proton abstraction for benzylamine is also reflected in $^{D}k_{cat}$, which is elevated relative to that of methylamine [$^{D}k_{cat}$(benzylamine) = 5.9, whereas $^{D}k_{cat}$(methylamine) = 1.7]. In previous studies of HPAO-1 with methylamine, three partially rate-determining steps have been documented that include aldehyde release, transfer of the first electron to oxygen, and hydrogen peroxide and/or ammonium release (*26*). Loss of a proton from C1 of the substrate Schiff base must contribute significantly to the decreased rate of turnover with benzylamine, since all steps after oxygen binding are common to both substrates, and therefore cannot account for the difference in turnover rates (Scheme 1).

Significantly, the differences in $k_{cat}/K_m(S)$ are not mirrored in $k_{cat}/K_m(O_2)$. The oxygen binding and reactivity sites, copper, and copper ligands on the two enzymes are structurally similar. All the residues that define the O_2 anteroom close to the copper are different between HPAO-1 and -2, but the nature of the area is still hydrophobic (Table S2 of the Supporting Information). This is true in other CAOs, where the residues are not conserved but the hydrophobic nature of the pocket is maintained (*22*, *32*, *42*, *43*). Hence, the kinetic and structural data suggest a modular structure for both HPAOs, in which changes at the amine substrate site are not propagated to the pocket where oxygen undergoes reaction. Furthermore, the similar $k_{cat}/K_m(O_2)$ values for both isoenzymes, regardless of substrate, support the ping-pong mechanism proposed for HPAO-1 (Scheme 1). The stark contrast between the substrate-dependent changes in $k_{cat}/K_m(S)$ and the substrate-independent $k_{cat}/K_m(O_2)$ highlights the independence of the oxygen binding and reduction sites from the structural determinants affecting amine kinetics.

CONCLUSIONS

In this study, we have investigated the origins of substrate specificity in the copper amine oxidases designated HPAO-1 and HPAO-2. From the newly determined crystal structure of HPAO-2 in comparison with that of HPAO-1, we can begin to see how the narrow binding channel of HPAO-1 may predispose that CAO isoenzyme to reaction with smaller aliphatic amines via changes in substrate binding energies. However, selection against the smaller aliphatic substrate in the wide funnel-like substrate binding channel of HPAO-2 cannot be due to sterics alone. A significant increase in $^{D}k_{cat}/K_m$ values for the poorer methylamine substrate relative to the preferred substrate indicates that proton abstraction has become rate-determining with this substrate. An impairment of the positioning of the methylamine substrate Schiff base in HPAO-2 affords the most likely explanation for the increase in $^{D}k_{cat}/K_m(S)$, while the reduction in the absolute magnitude of $k_{cat}/K_m(S)$ likely arises from numerous factors. Conversely, in HPAO-1, both binding of substrate and release of product, as well as the proton abstraction step, appear to be hindered under catalysis with the bulkier aromatic amine. This combination of kinetic and structural characterization reveals the multiplicity of factors that enters into the differential discrimination between large and small substrates at the active sites of a pair of paralogous enzymes catalyzing identical chemical reactions.

ACKNOWLEDGMENT

Computer resources were provided by the Basic Sciences Computing Laboratory of the University of Minnesota Supercomputing Institute, and we thank Can Ergenekan for his support. X-ray data were collected at the Kahlert Structural Biology Laboratory (KSBL) at The University of Minnesota and beamline 19-ID-D, SBC-CAT, at the Advanced Photon Source (APS), Argonne National Laboratory (Argonne, IL). The work was performed at Argonne National Laboratory, Structural Biology Center at the Advanced Photon Source. Argonne is operated by UChicago Argonne, LLC, for the U.S. Department of Energy, Office of Biological and Environmental Research, under Contract DE-AC02-06CH11357. We thank Ed Hoeffner for KSBL support and Steve Ginell and the staff at Sector 19, APS, for their support. We also thank Peder Cedervall and Brandon Goblirsch for help in the generation of figures and Rhein Biotech for the access to the *H. polymorpha* Genome Data Base.

SUPPORTING INFORMATION AVAILABLE

Comparison of k_{cat} values in EDTA-dialyzed versus nondialyzed HPAO-2 samples (Table S1), residue changes that define the O_2 anteroom (Table S2), HPAO-1 and HPAO-2 sequence alignment (Figure S1), 10% SDS−PAGE gel of HPAO-2 (Figure S2), comparison of the N-terminal sequence of HPAO-2 and HPAO-1 (Figure S3), stereo graphic of the $2F_o - F_c$ electron density quality in HPAO-2 (Figure S4), overall fold of the HPAO-2 dimer (Figure S5), ribbon diagrams showing an overlay of HPAO-1 and HPAO-2 (Figure S6), graphics of the side chamber located in the HPAO-2 entry channel (Figure S7), TPQ environment showing that only one face of the ring can support nucleophilic attack (Figure S8), and model of the product Schiff base of benzylamine with TPQ (Figure S9). This material is available free of charge via the Internet at http://pubs.acs.org.

REFERENCES

1. Mure, M., Mills, S. A., and Klinman, J. P. (2002) Catalytic mechanism of the topa quinone containing copper amine oxidases. *Biochemistry 41*, 9269–9278.
2. Parsons, M. R., Convery, M. A., Wilmot, C. M., Yadav, K. D., Blakeley, V., Corner, A. S., Phillips, S. E., McPherson, M. J., and Knowles, P. F. (1995) Crystal structure of a quinoenzyme: Copper amine oxidase of *Escherichia coli* at 2 Å resolution. *Structure 3*, 1171–1184.
3. Roh, J. H., Suzuki, H., Azakami, H., Yamashita, M., Murooka, Y., and Kumagai, H. (1994) Purification, Characterization, and Crystallization of Monoamine-Oxidase from *Escherichia coli* K-12. *Biosci., Biotechnol., Biochem. 58*, 1652–1656.
4. Cai, D. Y., and Klinman, J. P. (1994) Copper amine oxidase: Heterologous expression, purification, and characterization of an active enzyme in *Saccharomyces cerevisiae*. *Biochemistry 33*, 7647–7653.
5. Cronin, C. N., and Kirsch, J. F. (1988) Role of arginine-292 in the substrate specificity of aspartate aminotransferase as examined by site-directed mutagenesis. *Biochemistry 27*, 4572–4579.
6. Youdim, M. B., Edmondson, D., and Tipton, K. F. (2006) The therapeutic potential of monoamine oxidase inhibitors. *Nat. Rev. 7*, 295–309.
7. Kawaguchi, S., Nobe, Y., Yasuoka, J., Wakamiya, T., Kusumoto, S., and Kuramitsu, S. (1997) Enzyme flexibility: A new concept in recognition of hydrophobic substrates. *J. Biochem. 122*, 55–63.
8. Tsugeno, Y., and Ito, A. (1997) A key amino acid responsible for substrate selectivity of monoamine oxidase A and B. *J. Biol. Chem. 272*, 14033–14036.
9. Li, R. B., Klinman, J. P., and Mathews, F. S. (1998) Copper amine oxidase from *Hansenula polymorpha*: The crystal structure determined at 2.4 angstrom resolution reveals the active conformation. *Structure 6*, 293–307.
10. De Hoop, M. J., Valkema, R., Kienhuis, C. B., Hoyer, M. A., and Ab, G. (1992) The peroxisomal import signal of amine oxidase from the yeast *Hansenula polymorpha* is not universal. *Yeast 8*, 243–252.
11. Lander, E. S., Linton, L. M., Birren, B., Nusbaum, C., Zody, M. C., Baldwin, J., Devon, K., Dewar, K., Doyle, M., FitzHugh, W., Funke, R., Gage, D., Harris, K., Heaford, A., Howland, J., Kann, L., Lehoczky, J., LeVine, R., McEwan, P., McKernan, K., Meldrim, J., Mesirov, J. P., Miranda, C., Morris, W., Naylor, J., Raymond, C., Rosetti, M., Santos, R., Sheridan, A., Sougnez, C., Stange-Thomann, N., Stojanovic, N., Subramanian, A., Wyman, D., Rogers, J., Sulston, J., Ainscough, R., Beck, S., Bentley, D., Burton, J., Clee, C., Carter, N., Coulson, A., Deadman, R., Deloukas, P., Dunham, A., Dunham, I., Durbin, R., French, L., Grafham, D., Gregory, S., Hubbard, T., Humphray, S., Hunt, A., Jones, M., Lloyd, C., McMurray, A., Matthews, L., Mercer, S., Milne, S., Mullikin, J. C., Mungall, A., Plumb, R., Ross, M., Shownkeen, R., Sims, S., Waterston, R. H., Wilson, R. K., Hillier, L. W., McPherson, J. D., Marra, M. A., Mardis, E. R., Fulton, L. A., Chinwalla, A. T., Pepin, K. H., Gish, W. R., Chissoe, S. L., Wendl, M. C., Delehaunty, K. D., Miner, T. L., Delehaunty, A., Kramer, J. B., Cook, L. L., Fulton, R. S., Johnson, D. L., Minx, P. J., Clifton, S. W., Hawkins, T., Branscomb, E., Predki, P., Richardson, P., Wenning, S., Slezak, T., Doggett, N., Cheng, J. F., Olsen, A., Lucas, S., Elkin, C., Uberbacher, E., Frazier, M., Gibbs, R. A., Muzny, D. M., Scherer, S. E., Bouck, J. B., Sodergren, E. J.,

Worley, K. C., Rives, C. M., Gorrell, J. H., Metzker, M. L., Naylor, S. L., Kucherlapati, R. S., Nelson, D. L., Weinstock, G. M., Sakaki, Y., Fujiyama, A., Hattori, M., Yada, T., Toyoda, A., Itoh, T., Kawagoe, C., Watanabe, H., Totoki, Y., Taylor, T., Weissenbach, J., Heilig, R., Saurin, W., Artiguenave, F., Brottier, P., Bruls, T., Pelletier, E., Robert, C., Wincker, P., Smith, D. R., Doucette-Stamm, L., Rubenfield, M., Weinstock, K., Lee, H. M., Dubois, J., Rosenthal, A., Platzer, M., Nyakatura, G., Taudien, S., Rump, A., Yang, H., Yu, J., Wang, J., Huang, G., Gu, J., Hood, L., Rowen, L., Madan, A., Qin, S., Davis, R. W., Federspiel, N. A., Abola, A. P., Proctor, M. J., Myers, R. M., Schmutz, J., Dickson, M., Grimwood, J., Cox, D. R., Olson, M. V., Kaul, R., Raymond, C., Shimizu, N., Kawasaki, K., Minoshima, S., Evans, G. A., Athanasiou, M., Schultz, R., Roe, B. A., Chen, F., Pan, H., Ramser, J., Lehrach, H., Reinhardt, R., McCombie, W. R., de la Bastide, M., Dedhia, N., Blocker, H., Hornischer, K., Nordsiek, G., Agarwala, R., Aravind, L., Bailey, J. A., Bateman, A., Batzoglou, S., Birney, E., Bork, P., Brown, D. G., Burge, C. B., Cerutti, L., Chen, H. C., Church, D., Clamp, M., Copley, R. R., Doerks, T., Eddy, S. R., Eichler, E. E., Furey, T. S., Galagan, J., Gilbert, J. G., Harmon, C., Hayashizaki, Y., Haussler, D., Hermjakob, H., Hokamp, K., Jang, W., Johnson, L. S., Jones, T. A., Kasif, S., Kaspryzk, A., Kennedy, S., Kent, W. J., Kitts, P., Koonin, E. V., Korf, I., Kulp, D., Lancet, D., Lowe, T. M., McLysaght, A., Mikkelsen, T., Moran, J. V., Mulder, N., Pollara, V. J., Ponting, C. P., Schuler, G., Schultz, J., Slater, G., Smit, A. F., Stupka, E., Szustakowski, J., Thierry-Mieg, D., Thierry-Mieg, J., Wagner, L., Wallis, J., Wheeler, R., Williams, A., Wolf, Y. I., Wolfe, K. H., Yang, S. P., Yeh, R. F., Collins, F., Guyer, M. S., Peterson, J., Felsenfeld, A., Wetterstrand, K. A., Patrinos, A., Morgan, M. J., de Jong, P., Catanese, J. J., Osoegawa, K., Shizuya, H., Choi, S., and Chen, Y. J. (2001) Initial sequencing and analysis of the human genome. *Nature 409*, 860–921.

12. Elmore, B. O., Bollinger, J. A., and Dooley, D. M. (2002) Human kidney diamine oxidase: Heterologous expression, purification, and characterization. *J. Biol. Inorg. Chem. 7*, 565–579.
13. Marti, L., Abella, A., De La Cruz, X., Garcia-Vicente, S., Unzeta, M., Carpene, C., Palacin, M., Testar, X., Orozco, M., and Zorzano, A. (2004) Exploring the binding mode of semicarbazide-sensitive amine oxidase/VAP-1: Identification of novel substrates with insulin-like activity. *J. Med. Chem. 47*, 4865–4874.
14. Airenne, T. T., Nymalm, Y., Kidron, H., Smith, D. J., Pihlavisto, M., Salmi, M., Jalkanen, S., Johnson, M. S., and Salminen, T. A. (2005) Crystal structure of the human vascular adhesion protein-1: Unique structural features with functional implications. *Protein Sci. 14*, 1964–1974.
15. Jakobsson, E., Nilsson, J., Ogg, D., and Kleywegt, G. J. (2005) Structure of human semicarbazide-sensitive amine oxidase/vascular adhesion protein-1. *Acta Crystallogr. D61*, 1550–1562.
16. McGrath, A. P., Hilmer, K. M., Collyer, C. A., Shepard, E. M., Elmore, B. O., Brown, D. E., Dooley, D. M., and Guss, J. M. (2009) Structure and inhibition of human diamine oxidase. *Biochemistry 48*, 9810–9822.
17. DuBois, J. L., and Klinman, J. P. (2004) Methods for characterizing TPQ-containing proteins. *Methods Enzymol. 378*, 17−31.
18. Neumann, R., Hevey, R., and Abeles, R. H. (1975) The action of plasma amine oxidase on β-haloamines. Evidence for proton abstraction in the oxidative reaction. *J. Biol. Chem. 250*, 6362–6367.
19. Hartmann, C., and Klinman, J. P. (1991) Structure-function studies of substrate oxidation by bovine serum amine oxidase: Relationship to cofactor structure and mechanism. *Biochemistry 30*, 4605–4611.
20. Otwinowski, Z., and Minor, W. (1997) Processing of X-ray diffraction data collected in oscillation mode. *Methods Enzymol. 276*, 307–326.
21. Collaborative Computational Project, Number 4 (1994) The CCP4 suite: Programs for protein crystallography. *Acta Crystallogr. D50*, 760–763.
22. Johnson, B. J., Cohen, J., Welford, R. W., Pearson, A. R., Schulten, K., Klinman, J. P., and Wilmot, C. M. (2007) Exploring molecular oxygen pathways in *Hansenula polymorpha* copper-containing amine oxidase. *J. Biol. Chem. 282*, 17767–17776.
23. Emsley, P., and Cowtan, K. (2004) Coot: Model-building tools for molecular graphics. *Acta Crystallogr. D60*, 2126–2132.
24. Murshudov, G. N., Vagin, A. A., and Dodson, E. J. (1997) Refinement of macromolecular structures by the maximum-likelihood method. *Acta Crystallogr. D53*, 240–255.
25. Langer, G., Cohen, S. X., Lamzin, V. S., and Perrakis, A. (2008) Automated macromolecular model building for X-ray crystallography using ARP/wARP version 7. *Nat. Protoc. 3*, 1171–1179.
26. Takahashi, K., and Klinman, J. P. (2006) Relationship of stopped flow to steady state parameters in the dimeric copper amine oxidase from *Hansenula polymorpha* and the role of zinc in inhibiting activity at alternate copper-containing subunits. *Biochemistry 45*, 4683–4694.
27. Wilmot, C. M., Hajdu, J., McPherson, M. J., Knowles, P. F., and Phillips, S. E. (1999) Visualization of dioxygen bound to copper during enzyme catalysis. *Science 286*, 1724–1728.
28. Hevel, J. M., Mills, S. A., and Klinman, J. P. (1999) Mutation of a strictly conserved, active-site residue alters substrate specificity and cofactor biogenesis in a copper amine oxidase. *Biochemistry 38*, 3683–3693.
29. van Roermund, C. W., de Jong, M., Ijlst, L., van Marle, J., Dansen, T. B., Wanders, R. J., and Waterham, H. R. (2004) The peroxisomal lumen in *Saccharomyces cerevisiae* is alkaline. *J. Cell Sci. 117*, 4231–4237.
30. Duff, A. P., Cohen, A. E., Ellis, P. J., Kuchar, J. A., Langley, D. B., Shepard, E. M., Dooley, D. M., Freeman, H. C., and Guss, J. M. (2003) The crystal structure of *Pichia pastoris* lysyl oxidase. *Biochemistry 42*, 15148–15157.
31. Kumar, V., Dooley, D. M., Freeman, H. C., Guss, J. M., Harvey, I., McGuirl, M. A., Wilce, M. C., and Zubak, V. M. (1996) Crystal structure of a eukaryotic (pea seedling) copper-containing amine oxidase at 2.2 Å resolution. *Structure 4*, 943–955.
32. Lunelli, M., Di Paolo, M. L., Biadene, M., Calderone, V., Battistutta, R., Scarpa, M., Rigo, A., and Zanotti, G. (2005) Crystal structure of amine oxidase from bovine serum. *J. Mol. Biol. 346*, 991–1004.
33. Wilce, M. C. J., Dooley, D. M., Freeman, H. C., Guss, J. M., Matsunami, H., McIntire, W. S., Ruggiero, C. E., Tanizawa, K., and Yamaguchi, H. (1997) Crystal structures of the copper-containing amine oxidase from *Arthrobacter globiformis* in the holo and apo forms: Implications for the biogenesis of topaquinone. *Biochemistry 36*, 16116–16133.
34. De Biase, D., Agostinelli, E., De Matteis, G., Mondovi, B., and Morpurgo, L. (1996) Half-of-the-sites reactivity of bovine serum amine oxidase. Reactivity and chemical identity of the second site. *Eur. J. Biochem. 237*, 93–99.
35. Frebort, I., Toyama, H., Matsushita, K., and Adachi, O. (1995) Half-site reactivity with p-nitrophenylhydrazine and subunit separation of the dimeric copper-containing amine oxidase from *Aspergillus niger*. *Biochem. Mol. Biol. Int. 36*, 1207–1216.
36. Wilmot, C. M., Murray, J. M., Alton, G., Parsons, M. R., Convery, M. A., Blakeley, V., Corner, A. S., Palcic, M. M., Knowles, P. F., McPherson, M. J., and Phillips, S. E. (1997) Catalytic mechanism of the quinoenzyme amine oxidase from *Escherichia coli*: Exploring the reductive half-reaction. *Biochemistry 36*, 1608–1620.
37. Chiu, Y. C., Okajima, T., Murakawa, T., Uchida, M., Taki, M., Hirota, S., Kim, M., Yamaguchi, H., Kawano, Y., Kamiya, N., Kuroda, S., Hayashi, H., Yamamoto, Y., and Tanizawa, K. (2006) Kinetic and structural studies on the catalytic role of the aspartic acid residue conserved in copper amine oxidase. *Biochemistry 45*, 4105–4120.
38. Wilmot, C. M., Saysell, C. G., Blessington, A., Conn, D. A., Kurtis, C. R., McPherson, M. J., Knowles, P. F., and Phillips, S. E. (2004) Medical implications from the crystal structure of a copper-containing amine oxidase complexed with the antidepressant drug tranylcypromine. *FEBS Lett. 576*, 301–305.
39. Murray, J. M., Saysell, C. G., Wilmot, C. M., Tambyrajah, W. S., Jaeger, J., Knowles, P. F., Phillips, S. E. V., and McPherson, M. J. (1999) The Active Site Base Controls Cofactor Reactivity in *Escherichia coli* Amine Oxidase: X-ray Crystallographic Studies with Mutational Variants. *Biochemistry 38*, 8217–8227.
40. Schwartz, B., Green, E. L., Sanders-Loehr, J., and Klinman, J. P. (1998) Relationship between Conserved Consensus Site Residues and the Productive Conformation for the TPQ Cofactor in a Copper-Containing Amine Oxidase from Yeast. *Biochemistry 37*, 16591–16600.
41. Hartmann, C., and Klinman, J. P. (1991) Structure-function studies of substrate oxidation by bovine serum amine oxidase: Relationship to cofactor structure and mechanism. *Biochemistry 30*, 4605–4611.
42. Duff, A. P., Trambaiolo, D. M., Cohen, A. E., Ellis, P. J., Juda, G. A., Shepard, E. M., Langley, D. B., Dooley, D. M., Freeman, H. C., and Guss, J. M. (2004) Using xenon as a probe for dioxygen-binding sites in copper amine oxidases. *J. Mol. Biol. 344*, 599–607.
43. Pirrat, P., Smith, M. A., Pearson, A. R., McPherson, M. J., and Phillips, S. E. V. (2008) Structure of a xenon derivative of *Escherichia coli* copper amine oxidase: Confirmation of the proposed oxygen-entry pathway. *Acta Crystallogr. F64*, 1105–1109.